IOP Publishing Smart Materials and Structures
Smart Mater. Struct. **26** (2017) 055027 (9pp) https://doi.org/10.1088/1361-665X/aa688b

Magnetic flux biasing of magnetostrictive sensors

Zhangxian Deng and Marcelo J Dapino

NSF I/UCRC Smart Vehicle Concepts Center, Department of Mechanical and Aerospace Engineering, The Ohio State University, Columbus, OH 43210, United States of America

E-mail: dapino.1@osu.edu

Received 19 January 2017, revised 16 March 2017
Accepted for publication 22 March 2017
Published 19 April 2017

Abstract

The performance of magnetostrictive materials, especially those with high initial magnetic permeability and associated low magnetic reluctance, is sensitive to not just the amount of magnetic bias but also how the bias is applied. Terfenol-D and Galfenol have been characterized under constant magnetic field and constant magnetomotive force, which require active control. The application of a magnetic flux bias utilizing permanent magnets allows for robust magnetostrictive systems that require no active control. However, this biasing configuration has not been thoroughly investigated. This study presents flux density versus stress major loops of Terfenol-D and Galfenol at various magnetic flux biases. A new piezomagnetic coefficient d_{33}^{ϕ} is defined as the locally-averaged slope of flux density versus stress. Considering the materials alone, the maximum d_{33}^{ϕ} is 18.42 T GPa^{-1} and 19.53 T GPa^{-1} for Terfenol-D and Galfenol, respectively. Compared with the peak piezomagnetic coefficient d_{33}^{*} measured under controlled magnetic fields, the piezomagnetic coefficient d_{33}^{ϕ} is 26% and 74% smaller for Terfenol-D and Galfenol, respectively. This study shows that adding parallel magnetic flux paths to low-reluctance magnetostrictive components can partially compensate for the performance loss. With a low carbon steel flux path in parallel to the Galfenol specimen, the maximum d_{33}^{ϕ} increased to 28.33 T GPa^{-1} corresponding to a 45% improvement compared with the case without a flux path. Due to its low magnetic permeability, Terfenol-D does not benefit from the addition of a parallel flux path.

Keywords: magnetostriction, Terfenol-D, Galfenol, d_{33} coefficient

(Some figures may appear in colour only in the online journal)

1. Introduction

Magnetostrictive terbium-iron-dysprosium, or Terfenol-D, exhibits a high magnetostriction of 1600×10^{-6} [1] and a moderate saturation magnetization of 630 kA m^{-1} [2]. Terfenol-D is brittle in tension (tensile strength ≈28 MPa) and thus it must be operated in pure compression or in complicated protection mechanisms to avoid cracking [2]. Terfenol-D exhibits a small relative magnetic permeability ranging from 2 to 10 [3] and a large magnetic field (over 100 kA m^{-1}) is required to fully saturate the material. Iron–gallium alloys, or Galfenol, exhibit a moderate magnetostriction of 350×10^{-6} [4] and a saturation magnetization of 1200 kA m^{-1} [5–7]. Galfenol is mechanically robust (tensile strength ≈500 MPa) [8]; it can be processed by conventional means, and deposited onto micro-scale films [9, 10]. The relative permeability of Galfenol ranges from 1 to 700 [11], thus requiring a much smaller magnetic excitation (⩽15 kA m^{-1}). Due to the strong magneto-mechanical coupling, Terfenol-D and Galfenol have been implemented in sensing [12], actuation [13], energy harvesting [14–16], and vibration control [17, 18].

The performance of magnetostrictive materials depends on the coupling of magnetic and mechanical energies. For a small stress perturbation ΔT and a small magnetic field perturbation ΔH, the constitutive behavior of

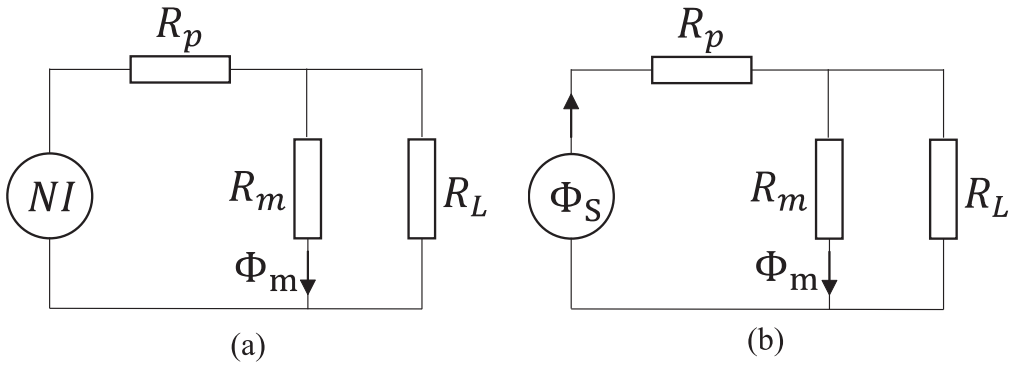

Figure 1. Equivalent electrical circuit for magnetostrictive systems under: (a) current bias and (b) permanent magnet bias.

magnetostrictive materials can be represented by

$$\Delta B = d_{33}^{*}\Delta T + \mu^{T}\Delta H \quad \text{and} \quad \Delta\lambda = \frac{1}{E^{H}}\Delta T + d_{33}^{*}\Delta H, \tag{1}$$

where $\Delta\lambda$ is the magnetostriction increment, ΔB is the increment of magnetic flux density. The magnetic permeability and Young's modulus at constant stress and constant magnetic field are μ^{T} and E^{H}, respectively. The piezomagnetic coefficient d_{33}^{*} can be approximately characterized either from magnetostriction versus magnetic field curves or from flux density versus stress curves as

$$d_{33}^{*} \triangleq \mathrm{d}\lambda/\mathrm{d}H = \mathrm{d}B/\mathrm{d}T. \tag{2}$$

The magnetic field in active magnetostrictive systems is usually generated via electromagnets. The values of d_{33}^{*} have been measured for Terfenol-D and Galfenol under static magnetic fields. Moffett *et al* [1] first characterized stress- and field-dependence of d_{33}^{*} in monolithic Terfenol-D by measuring magnetostriction versus magnetic field major loops under various mechanical loadings. Kellogg and Flatau [2] later measured the flux density versus stress major loops of Terfenol-D under constant magnetic fields. Galfenol with various compositions and crystal structures has been characterized in literature. Flux density versus stress major loops and d_{33}^{*} were measured for single crystal Galfenol at 18.9%, 24.7%, and 16% gallium [19, 20] under various static magnetic fields. Atulasimha *et al* [21] measured the flux density versus stress major loops of a polycrystalline $Fe_{81.6}Ga_{18.4}$ specimen and evaluated its d_{33}^{*} at controlled magnetic fields under varying compressions. Mahadevan *et al* [7] later extended the applied stress to tension and reported d_{33}^{*} measurements of polycrystalline $Fe_{81.6}Ga_{18.4}$ under constant tensile loadings.

For certain applications in which active magnetic field control is not possible, the piezomagnetic coefficients have been characterized at the system level by applying constant driving current to the electromagnets. The equivalent circuit for a magnetostrictive system with a bias current is presented in figure 1(a) and the corresponding piezomagnetic coefficient is defined as

$$d_{33}^{I} \triangleq \frac{\mathrm{d}B}{\mathrm{d}T} = \frac{NIR_L}{A_m}\frac{R_m(\bar{T})}{[R_m(\bar{T})(R_L+R_p)+R_LR_p]^2}\frac{\mathrm{d}R_m(T)}{\mathrm{d}T}, \tag{3}$$

where N is the total number of turns in the electromagnet, I is the constant driving current applied, A_m is the cross section of the magnetostrictive specimen, R_p is the magnetic reluctance of the flux path, A_m is the cross section of the magnetostrictive specimen, $\bar{T}$ is the average stress, $R_m(T)$ is the stress-dependent magnetic reluctance of the magnetostrictive component, and R_L is the magnetic reluctance of the flux leakage path. Restorff *et al* [22] first characterized d_{33}^{I} of polycrystalline $Fe_{81.6}Ga_{18.4}$ under varying compressive loadings. Weng *et al* [6] later analyzed the influence of stress amplitudes on d_{33}^{*} and d_{33}^{I} by comparing major and minor flux density versus stress loops. The rate-dependence of d_{33}^{I} has also been investigated. Scheidler *et al* [23] have recently characterized flux density versus stress loops up to 1 kHz.

Biasing with a current or magnetic field requires an electromagnetic drive and a controller, which adds cost and complexity to systems that require a small energy footprint such as energy harvesters [24, 25] and sensors. This study experimentally measures the flux density versus stress major loops of magnetostrictive materials under a fixed magnetic flux bias generated by permanent magnets. As shown in figure 1(b), the flux through the magnetostrictive specimen is

$$\Phi_m = \Phi_s\frac{R_L}{R_m(T)+R_L}. \tag{4}$$

The permanent magnets are simplified as a constant current source $\Phi_s = B_sA_s$, where B_s and A_s are the remanent flux density and the cross section of the permanent magnets, respectively. The constant-flux piezomagnetic coefficient is defined as

$$d_{33}^{\phi} \triangleq \frac{\mathrm{d}B}{\mathrm{d}T} = \frac{\Phi_s}{A_m}\frac{R_L}{(R_m(\bar{T})+R_L)^2}\frac{\mathrm{d}R_m}{\mathrm{d}T}. \tag{5}$$

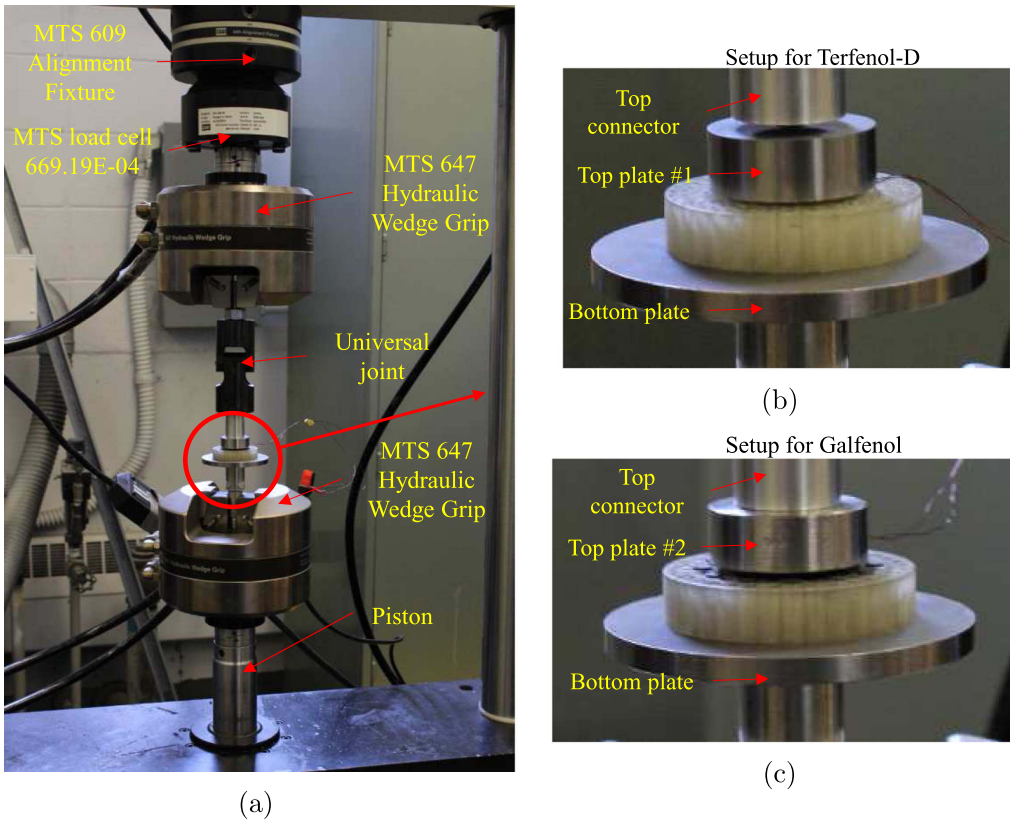

Figure 2. (a) Overall view of the load frame; (b) for Terfenol-D, the top plate is not attached to the top connector, whereas for Galfenol, a threaded stud connects the top plate and the top connector as shown in (c).

This article first presents flux density versus stress measurements obtained at various fixed magnetic flux biases for Terfenol-D and ⟨100⟩-oriented, highly textured, polycrystalline $Fe_{81.6}Ga_{18.4}$. A given flux bias is obtained by arranging a set of permanent magnets in a specified configuration. The dependence of the piezomagnetic coefficient d_{33}^{ϕ} on stress and field is determined from the data. Finally, this study validates the performance enhancement obtained by adding flux paths in parallel to magnetostrictive components.

2. Experimental setup

The measurements were conducted on two materials: Terfenol-D ($Tb_{0.3}Dy_{0.7}Fe_2$) and research grade, highly-textured, ⟨100⟩-oriented, polycrystalline Galfenol ($Fe_{81.6}Ga_{18.4}$). Both specimens are 6 mm in diameter and 10 mm in height. As shown in figure 2, the mechanical load was generated by an MTS 831.10 Elastomer Test System hydraulic load frame. The axial load applied on the specimen was measured by an MTS 661.19E-04 load cell. To ensure that the mechanical load on the specimen was purely compressive, a universal joint was added in between the top connector and the wedge grip. Further, all contact surfaces in the load path were ground. Fuji pressure measurement films [26] were used to ensure an even stress distribution on the contact surface.

The samples and surrounding components are shown in figures 3 and 4. Both top and bottom plates were made of magnetically-conductive stainless steel A430 such that flux leakage through surrounding air was minimized. A 500-turn pickup coil made of American Wire Gauge 30 copper wires was wound around the specimen. The coil dimensions have been determined in a previous study in order to maximize magneto-electrical coupling [27]. The output voltage from the pickup coil was routed to a Lakershore 480AH2 fluxmeter.

The desired range of magnetic flux biasing Φ_s has been determined for Terfenol-D and Galfenol using the numerical model presented in [27]. Varying Φ_s can be achieved either by changing the magnet geometry A_s or tuning the magnet strength B_s. Customizing cylindrical permanent magnets into desirable geometries can be difficult and costly. Instead, in this study a group of magnet stacks was arranged circumferentially as shown in figure 5. The axisymmetric permanent magnet arrangement ensures uniform magnetic field distribution in the magnetostrictive elements. A 3D-printed plastic magnet holder held the permanent magnets in place. The choice of B_s was determined based on the magnetic properties of magnetostrictive materials. Terfenol-D has a relatively small permeability and is less sensitive than Galfenol to magnetic field variation, and thus strong neodymium magnet stacks with a diameter of 0.125 inch (3.175 mm) and a height of 0.35 inch (8.89 mm) were used. Galfenol, on the other hand, has a relatively large permeability and thus moderate magnets (Alnico) with a diameter of 0.125 inch

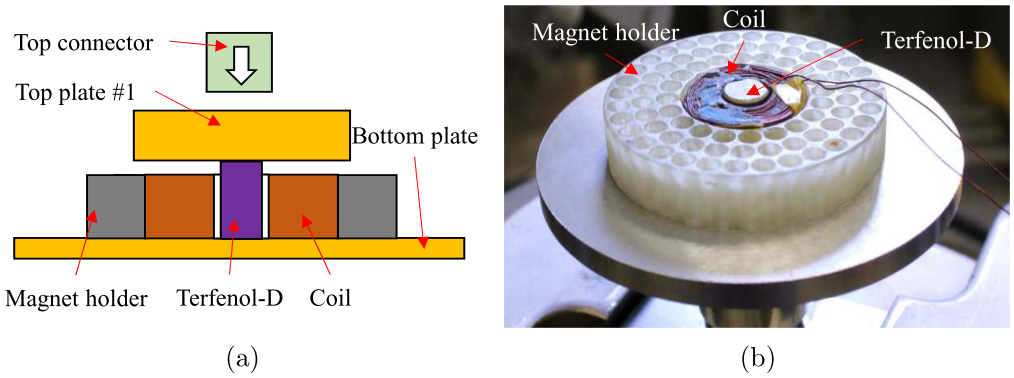

Figure 3. Experimental setup for Terfenol-D specimen: (a) schematics (before compression starts) and (b) physical setup.

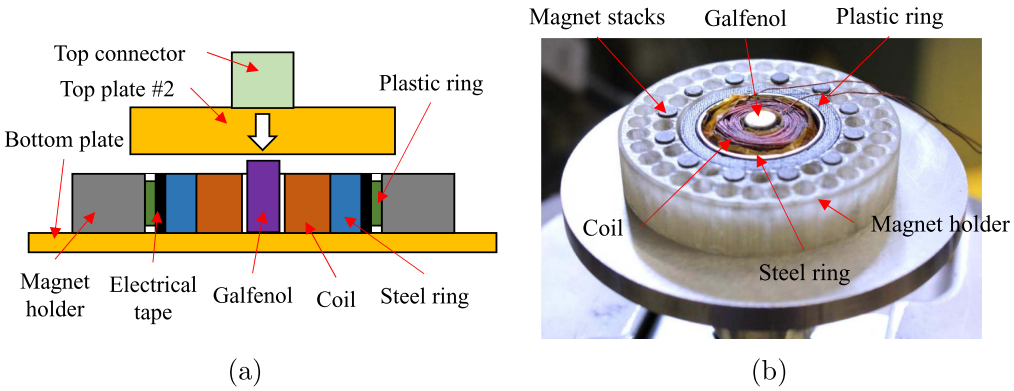

Figure 4. Experimental setup for Galfenol specimen: (a) schematics (before compression starts) and (b) physical setup.

(3.175 mm) and a height of 0.375 inch (9.525 mm) were used. The nominal remanent flux densities for neodymium magnets, Alnico grade 8 magnets, and Alnico grade 5 magnets are 1.23 T, 0.36 T, and 0.11 T, respectively. As detailed in section 3, these permanent magnet arrangements are suitable for investigating d_{33}^{ϕ} for both Terfenol-D and Galfenol.

The magnetic force F_m established between the magnetically-conductive top plate and the permanent magnets creates two challenges. The first challenge is that F_m tends to tilt the universal joint away from the vertical direction. Due to the strong neodymium magnets implemented in the Terfenol-D experiments, the maximum F_m could reach approximately 300 N. The influence of F_m on the spherical seat was completely eliminated by initially sitting the top plate on top of the specimen and shielding magnetic flux from the top connector, as shown in figure 3(a). However, the stress distribution was measured indirectly by inserting Fuji pressure measurement films between the top plate and the top connector. For the Galfenol experiments, the magnetic force is less than 50 N. Hence, the top plate was threaded into the top connector, as shown in figure 4(a). In this case, the stress distribution was evaluated directly on the top surface of the specimen. Vertical alignment was achieved by manually adjusting the top plate.

The second challenge is that the magnetic force affects force measurements thus being a source of error. The force reading on the load cell F_r includes the mechanical load applied on the sample F_s and F_m

$$F_r = -F_s + F_m. \tag{6}$$

The top plate was threaded to the top connector to calibrate F_m for both Terfenol-D and Galfenol. A typical force measurement observed during magnetic force calibration is shown in figure 6. The load cell was first tared when the top plate and the permanent magnets were far apart. The piston was then slowly raised. The value of F_r increased monotonically as the permanent magnets approached the top plate. Once the specimen touched the top platen, F_r started to decrease and the maximum F_r recorded was considered as F_m. All the data presented in this paper was adjusted to compensate for the effect of the magnetic force F_m.

Besides mechanical loads and magnetic fields, d_{33}^{ϕ} depends on the effective reluctance of the magnetic path in parallel to the specimen. Figure 1(b) presents an equivalent circuit that describes the magnetostrictive systems in figures 3 and 4. The corresponding d_{33}^{ϕ} is calculated in (5). The value of $\mathrm{d}R_m/\mathrm{d}T$ is a material property which only depends on input magnetic field and stress. Hence, the value of d_{33}^{ϕ} reaches a maximum when $R_L = R_m(\bar{T})$. For the Terfenol-D setup, R_L approximately equals the reluctance of the air gap in between the specimen and the permanent magnets. The permeability of Terfenol-D in the burst region ranges from 2 to 10 and thus $R_m(T)$ is intrinsically close to R_L. The relative permeability of Galfenol in the burst region ranges between 300 and 700, which is significant larger than the permeability of air. Hence,

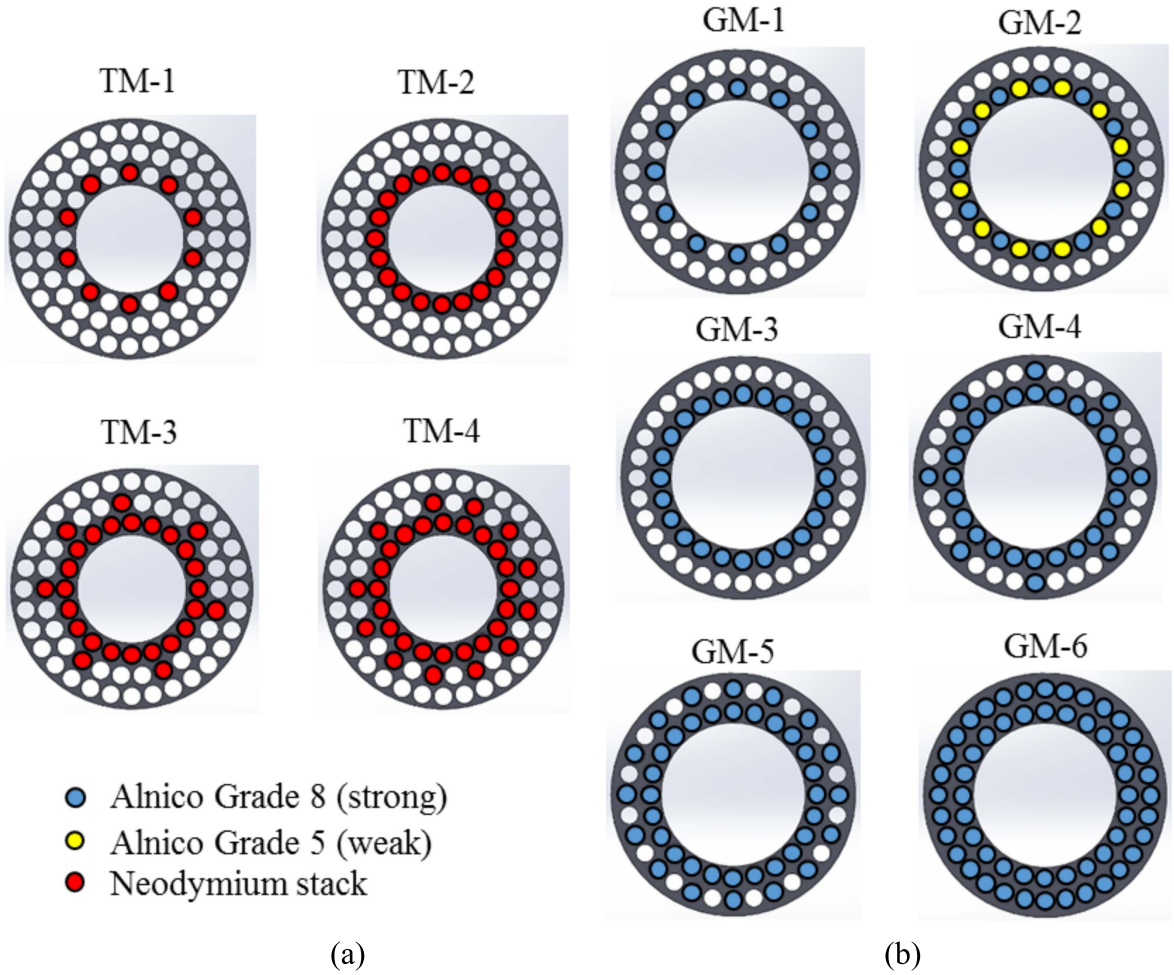

Figure 5. Permanent magnet configurations for (a) Terfenol-D setup and (b) Galfenol setup.

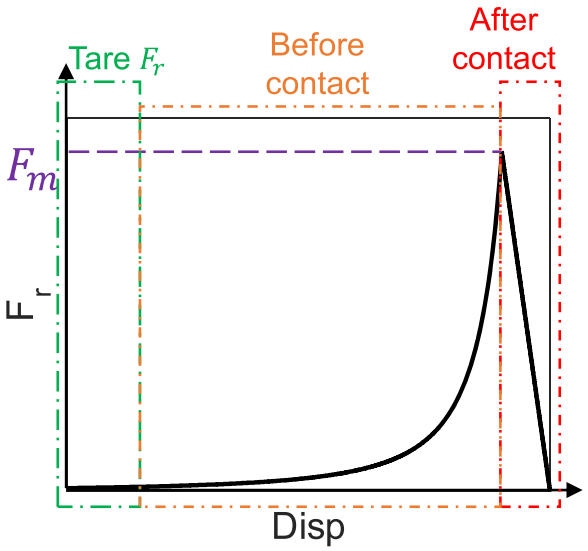

Figure 6. Force measured on the load cell versus piston displacement.

an additional steel ring in parallel to the Galfenol rod is necessary to provide a relatively low R_L. In this study, five 9.5 mm long 1018 low carbon steel rings, as shown in table 1, were tested. An electrical tape layer and a 3D printed plastic ring were squeezed in between the steel ring and the magnets, as shown in figure 4, to ensure concentric specimen and magnets alignment.

Table 1. Dimensions of the steel ring tested in this study.

Configuration no.	P1	P2	P3	P4	P5
Inner diameter (mm)	18.82	18.95	19.05	18.95	19.00
Wall thickness (mm)	0.5	1	1.5	2.5	3

This study applied a 0.5 Hz, 900 N amplitude sinusoidal force superimposed by a 1000 N DC compression to the magnetostrictive specimens. The excitation frequency is much smaller than the estimated cut-off frequency (≈112 Hz) [28], thus the eddy currents in the specimen are assumed to be negligible.

3. Results

3.1. Terfenol-D

Two observations are made from the Terfenol-D specimen: (1) the magnetic flux density decreases with increasing mechanical compression and (2) the magnetomechanical

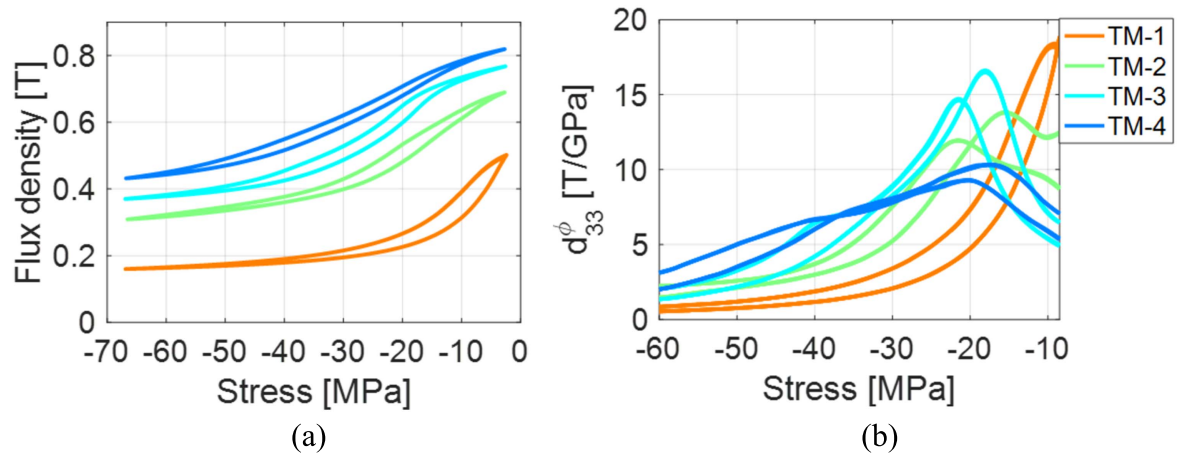

Figure 7. Experimental results of the Terfenol-D specimen: (a) flux density versus stress major loops and (b) piezomagnetic coefficient d_{33}^{ϕ} versus applied stress.

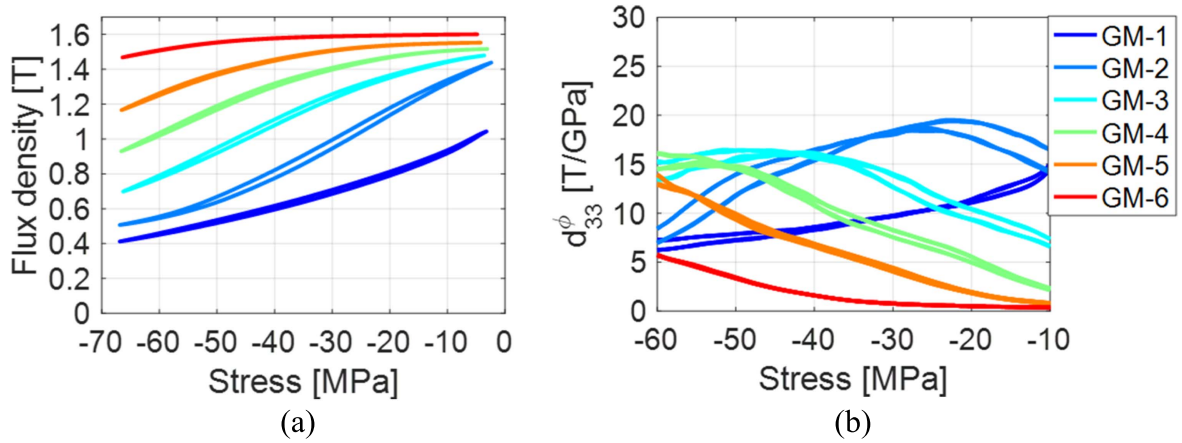

Figure 8. Experimental results of the Galfenol specimen without steel flux path: (a) flux density versus stress major loops and (b) piezomagnetic coefficient d_{33}^{ϕ} versus applied stress.

coupling under magnetic flux biasing is much weaker than under magnetic field biasing. Figure 7(a) shows flux density versus stress major loops under the four different permanent magnet configurations shown in figure 5(a). As the compressive stress increases, magnetic moments rotate toward directions which are perpendicular to the compression, and thus reduce magnetic flux density in the Terfenol-D specimen.

Regarding the reduction in magnetomechanical coupling, the piezomagnetic coefficient d_{33}^{ϕ} is calculated from -60 to -8.5 MPa. To mitigate the noise amplification from numerical differentiation, small sections (120 data points) of each curve are fit by 4th order polynomials, which are then analytically differentiated and evaluated at the center of each section. Figure 7(b) shows that a maximum d_{33}^{ϕ} of 18.42 T GPa^{-1} is achieved for the TM-1 magnet configuration and the optimal compressive stress is -9.15 MPa. Both flux density versus stress major loops and d_{33}^{ϕ} versus stress curves exhibit significant hysteresis. Without magnetic field control, an increasing mechanical compression reduces the magnetic permeability of magnetostrictive materials and then causes increasing magnetic field, which prevents magnetic domain rotation [11]. Hence, the flux density variation and the corresponding piezomagnetic coefficient become less significant when the magnetic field is not controlled to be constant. Compared to previous d_{33}^{*} measurement of Terfenol-D at static magnetic field [1], the maximum value of d_{33}^{ϕ} obtained in this study is 26% smaller.

The magnetomechanical coupling in Terfenol-D can possibly be improved by optimizing the dimension of the air gap. As shown in figure 3, the magnetic reluctance of the air gap between the permanent magnets and the Terfenol-D rod is R_{air} and thus $R_L = R_{\text{air}}$. By adjusting the air gap so that $R_L = R_{\text{air}} = R_m$, the piezomagnetic coefficient d_{33}^{ϕ} reaches the maximum value,

$$d_{33}^{\phi}|_{\text{Terfenol}} \approx \frac{\Phi_s}{A_m}\frac{\mathrm{d}R_m}{\mathrm{d}T}\frac{1}{4R_{\text{air}}} = \frac{\Phi_s}{A_m}\frac{\mathrm{d}R_m}{\mathrm{d}T}\frac{1}{4R_m}. \tag{7}$$

3.2. Galfenol—without flux path

The d_{33}^{ϕ} values of Galfenol were calculated using the same 4th order polynomial approximation. Figure 8(a) presents flux density versus stress major loops for the different permanent

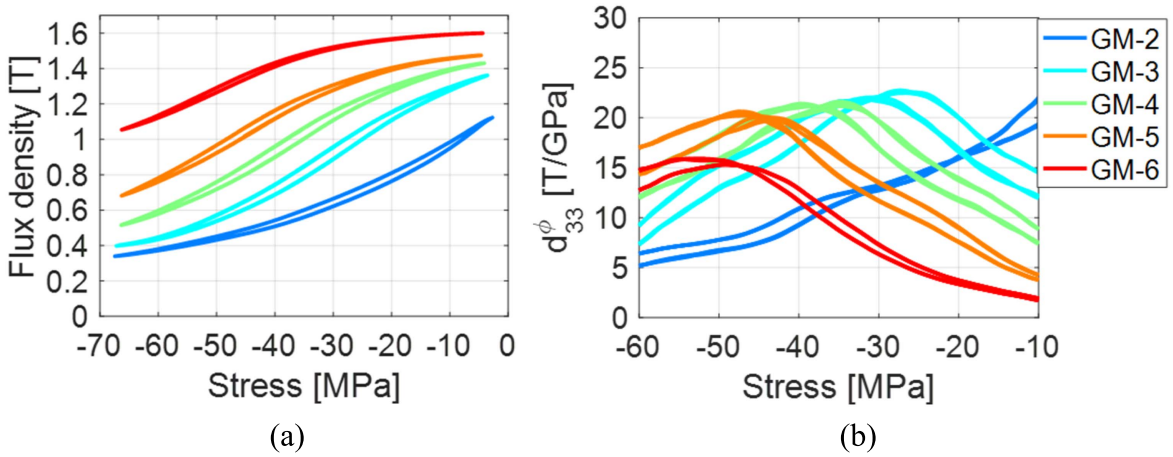

Figure 9. Experimental results of the Galfenol specimen with a steel ring of 0.5 mm wall thickness (P1): (a) flux density versus stress major loops and (b) piezomagnetic coefficient d_{33}^{ϕ} versus applied stress.

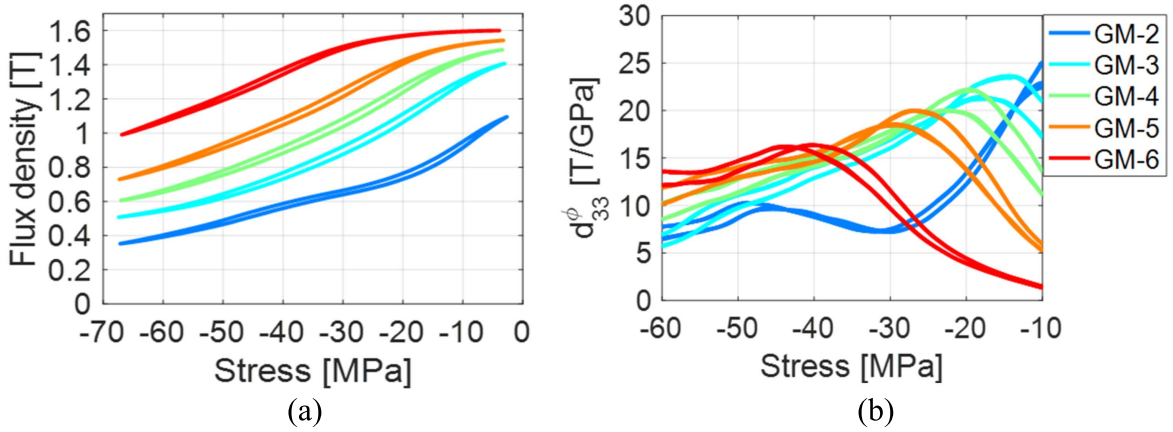

Figure 10. Experimental results of the Galfenol specimen with a steel ring of 1.0 mm wall thickness (P2): (a) flux density versus stress major loops and (b) piezomagnetic coefficient d_{33}^{ϕ} versus applied stress.

magnet configurations shown in figure 5(b). Figure 8(b) shows the d_{33}^{ϕ} versus stress curves of the Galfenol specimen when no flux paths (steel rings) were utilized. As the strength of the magnetic flux bias increases, the peak location of d_{33}^{ϕ} shifts to a higher compression and the peak value decreases. This trend indicates that larger mechanical energy is required to balance the increasing magnetic energy [6]. For the magnet configuration GM-3 and a compressive load of −23.04 MPa, the maximum value of d_{33}^{ϕ} is 19.53 T GPa^{-1}, which is 74% and 52% smaller than the previous d_{33}^{*} and d_{33}^{I} measurements, respectively [6]. Unlike the results measured from the Terfenol-D specimen, the peak locations and values change monotonically, as the magnet strength increases.

As shown in figure 4, $R_m \ll R_{\text{air}}$ and the magnetic flux provided by the permanent magnets always prefers to flow through the Galfenol rod. Hence, the flux variation in Galfenol and the corresponding piezomagnetic coefficient are very small.

3.3. Galfenol—with flux path

A previous numerical study on this setup has theoretically proven that a flux path in parallel to the Galfenol specimen is able to enhance the magnetomechanical coupling strength [27]. Assuming no additional flux paths are employed and recognizing $R_m \ll R_{\text{air}}$, the piezomagnetic coefficient defined in (5) can be simplified as

$$d_{33}^{\phi}|_{\text{no path}} \approx \frac{\Phi_s}{A_m}\frac{\mathrm{d}R_m}{\mathrm{d}T}\frac{1}{R_{\text{air}}}. \tag{8}$$

When a magnetically-conductive flux path is placed in the air gap, the value of R_L is dominated by the flux path. For the optimal flux path, or $R_L = R_m$, the piezomagnetic coefficient is maximum

$$d_{33}^{\phi}|_{\text{path}} \approx \frac{\Phi_s}{A_m}\frac{\mathrm{d}R_m}{\mathrm{d}T}\frac{1}{4R_m}. \tag{9}$$

Since R_m is much smaller than R_{air}, $d_{33}^{\phi}|_{\text{path}} > d_{33}^{\phi}|_{\text{no path}}$. In other words, adding a magnetic flux bypass improves the effective magnetomechanical coupling of Galfenol.

This study experimentally validates the contribution of flux paths in Galfenol-based systems by testing 5 different steel rings, as shown in table 1, which were inserted in parallel to the Galfenol rod. Figures 9–13 show that the peak of d_{33}^{ϕ} first increases as the thickness of the steel ring increases. The peak of d_{33}^{ϕ} along with the associated optimal magnetic

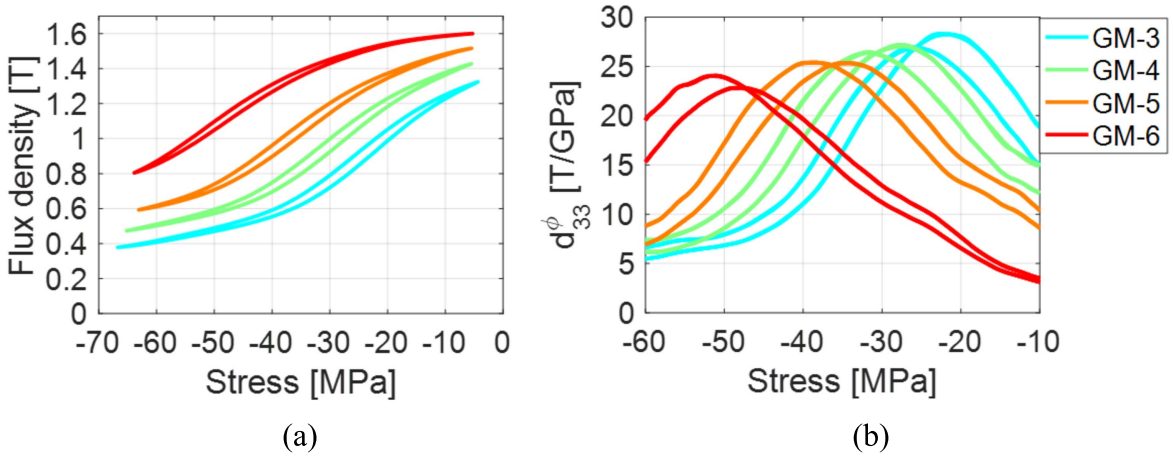

Figure 11. Experimental results of the Galfenol specimen with a steel ring of 1.5 mm wall thickness (P3): (a) flux density versus stress major loops and (b) piezomagnetic coefficient d_{33}^{ϕ} versus applied mechanical stress.

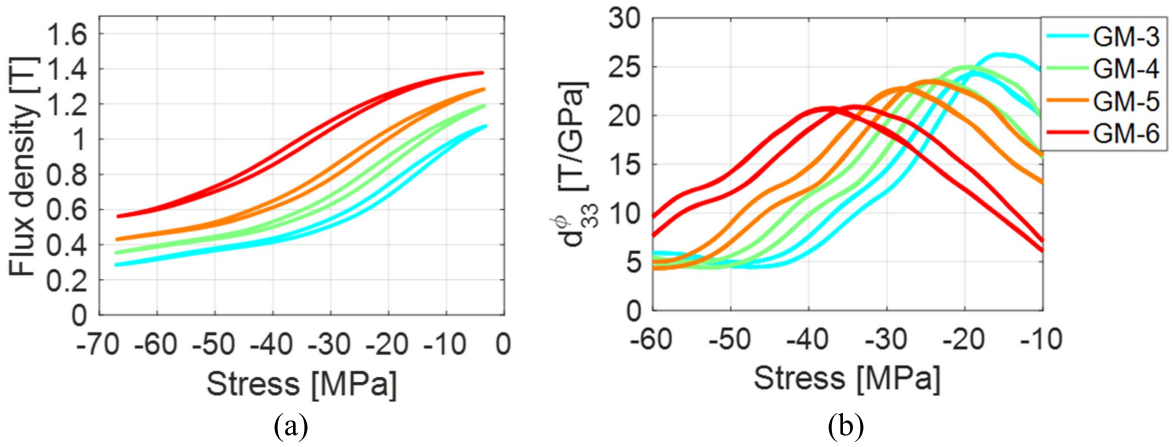

Figure 12. Experimental results of the Galfenol specimen with a steel ring of 2.5 mm wall thickness (P4): (a) flux density versus stress major loops and (b) piezomagnetic coefficient d_{33}^{ϕ} versus applied stress.

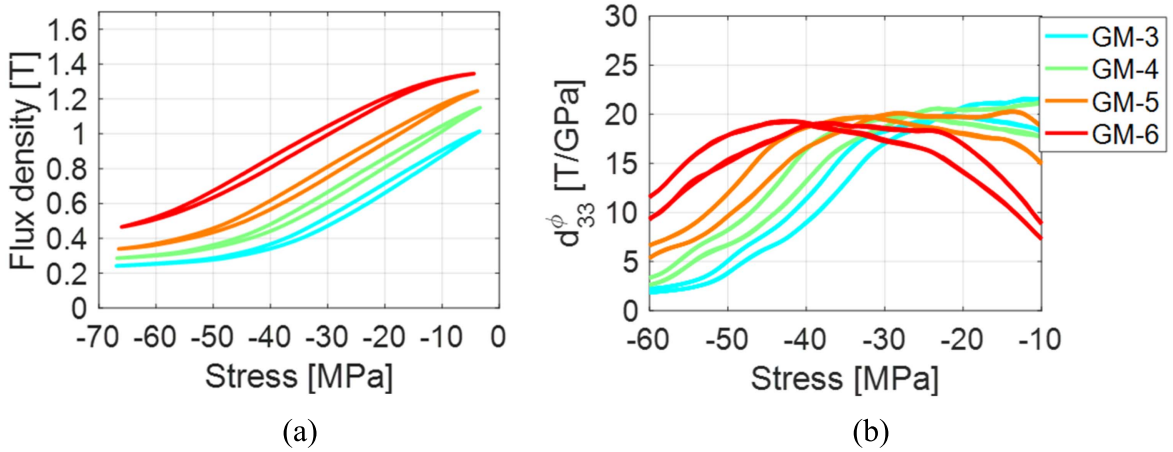

Figure 13. Experimental results of the Galfenol specimen with a steel ring of 3.0 mm wall thickness (P5): (a) flux density versus stress major loops and (b) piezomagnetic coefficient d_{33}^{ϕ} versus applied stress.

and mechanical biases are summarized in table 2 for different flux path configurations. The d_{33}^{ϕ} reaches the maximum value of 28.33 T GPa^{-1}, when the GM-3 magnet configuration, a compression stress of -21.53 MPa, and the steel ring P3 were implemented. The maximum d_{33}^{ϕ} of Galfenol was improved by 45% compared with the case without the flux path. As the wall thickness keeps increasing, more magnetic flux leaks through the steel ring and thus the peak of d_{33}^{ϕ} reduces. This

Table 2. The peak of d_{33}^{ϕ} and the associated optimal biases under different flux path configurations.

Flux path no.	No flux path	P1	P2	P3	P4	P5
Optimal stress (MPa)	−23.04	−27.30	−10.05	−21.53	−15.76	−12.16
Optimal magnet configuration	GM-3	GM-3	GM-2	GM-3	GM-3	GM-3
Max. d_{33}^{ϕ} (T GPa^{-1})	19.53	22.75	25.09	28.33	26.72	21.54

result experimentally proves that adding parallel magnetic flux paths to low-reluctance magnetostrictive components can partially compensate for the performance loss.

4. Concluding remarks

Piezomagnetic coefficients in Terfenol-D and Galfenol have been characterized under constant magnetic field and constant magnetomotive force, which require active control. Magnetic flux bias, which is usually provided by permanent magnets allows for compact, efficient, and robust magnetostrictive systems including energy harvesters, vibration dampers, and sensors. However, the performance of magnetostrictive materials under magnetic flux bias has not been thoroughly investigated. This study for the first time characterized the dependence of piezomagnetic coefficient d_{33}^{ϕ} on applied stress and magnetic field for Terfenol-D and Galfenol under various magnetic flux biases. The piezomagnetic coefficient d_{33}^{ϕ}, which approximately describes the magneto-mechanical coupling in magnetostrictive materials under magnetic flux bias, decreases significantly in both Terfenol-D and Galfenol. The maximum d_{33}^{ϕ} of Terfenol-D is 18.42 T GPa^{-1}, which is 26% smaller than the maximum piezomagnetic coefficient measured under constant magnetic field. The maximum d_{33}^{ϕ} of Galfenol is 19.53 T GPa^{-1}, which is 74% and 52% smaller than the values obtained under constant magnetic field and constant magnetomotive force, respectively. Appropriate flux path design is able to partially compensate for the performance loss. By attaching a 1.5 mm thick low carbon steel ring in parallel to the Galfenol specimen, the maximum d_{33}^{ϕ} increases to 28.33 T GPa^{-1} corresponding to a 45% enhancement. However, this method is not valid for Terfenol-D whose reluctance is large. The air surrounding the Terfenol-D specimen intrinsically operates as a flux path and the size of the air gap needs to be carefully designed for passive Terfenol-D systems.

Acknowledgments

We wish to acknowledge the member organizations of the Smart Vehicle Concepts Center, a National Science Foundation Industry/University Cooperative Research Center (www.SmartVehicleCenter.org) established under NSF Grant IIP-1238286.

References

[1] Moffett M B, Clark A E, Wun-Fogle M, Linberg J, Teter J P and McLaughlin E A 1991 *J. Acoust. Soc. Am.* **89** 1448–55
[2] Kellogg A and Flatau A B 2008 *J. Intell. Mater. Syst. Struct.* **19** 583–95
[3] http://tdvib.com/terfenol-d/
[4] Clark A E, Wun-Fogle M, Restorff J B and Lograsso T A 2002 *Mater. Trans.* **43** 881–6
[5] Atulasimha J and Flatau A B 2011 *Smart Mater. Struct.* **20** 043001
[6] Weng L, Walker T, Deng Z, Dapino M J and Wang B 2013 *J. Appl. Phys.* **113** 024508
[7] Mahadevan A, Evans P G and Dapino M J 2010 *Appl. Phys. Lett.* **96** 012502
[8] Nolting A E and Summers E 2015 *J. Mater. Sci.* **50** 5136–44
[9] Wenzel C, Adolphi B, Merkel U, Jahn A, Marschner U, Ziske J, Neubert H and Fischer W J 2009 *Sensors Actuators A* **156** 129–33
[10] Sauer S, Marschner U, Adolphi U, Clasbrummel B and Fischer W 2012 *IEEE Sens. J.* **12** 1226–33
[11] Deng Z and Dapino M J 2014 *J. Intell. Mater. Syst. Struct.* **26** 47–55
[12] Dapino M J, Deng Z, Calkins F T and Flatau A B 2016 *Wiley Encyclopedia of Electrical and Electronics Engineering* (New York: Wiley) (https://doi.org/10.1002/047134608X.W4549.pub2)
[13] Huang W, Wang B, Yan R, Cao S, Weng L and Yan W 2005 A numerical dynamic model of giant magnetostrictive actuator *2005 ICEMS* vol 1, pp 772–4
[14] Deng Z and Dapino M J 2015 *Smart Mater. Struct.* **24** 125019
[15] Ueno T and Yamada S 2011 *IEEE Trans. Magn.* **47** 2407–9
[16] Staley M E and Flatau A B 2005 *Proc. SPIE* **5764** 630–40
[17] Asnani V M, Deng Z, Scheidler J J and Dapino M J 2016 *Proc. SPIE* **9801** 98010R
[18] Yoo J H, Murray A and Flatau A B 2014 *Proc. SPIE* **9057** 90573I
[19] Atulasimha J and Flatau A B 2008 *J. Intell. Mater. Syst. Struct.* **19** 1371–81
[20] Datta S, Atulasimha J and Flatau A B 2009 *J. Magn. Magn. Mater.* **321** 4017–31
[21] Atulasimha J, Flatau A B and Summers E 2007 *Smart Mater. Struct.* **16** 1265
[22] Restorff J B, Wun-Fogle M and Summers E 2011 *J. Appl. Phys.* **109** 07A922
[23] Scheidler J J, Asnani V M and Dapino M J 2016 *J. Appl. Phys.* **119** 244902
[24] Berbyuk V and Sodhani J 2008 *Comput. Struct.* **86** 307–13
[25] Berbyuk V 2013 *Proc. SPIE* **8688** 86881F
[26] http://fujifilm.com/products/prescale/
[27] Deng Z, Asnani V M and Dapino M J 2015 *Proc. SPIE* **9433** 94330C
[28] Scheidler J J and Dapino M J 2016 *J. Magn. Magn. Mater.* **397** 233–9